arXiv:1407.0959v1 [quant-ph] 3 Jul 2014

Efficient algorithm for optimizing data pattern tomography

L. Motka,[1] B. Stoklasa,[1] J. Rehacek,[1] Z. Hradil,[1] V. Karasek,[1]
D. Mogilevtsev,[2] G. Harder,[3] C. Silberhorn,[3,4] and L. L. Sánchez-Soto[4,5]

[1]*Department of Optics, Palacky University, 17. listopadu 12, 77146 Olomouc, Czech Republic*
[2]*Institute of Physics, Belarus National Academy of Sciences, F Skarina Ave 68, Minsk 220072, Belarus*
[3]*Department of Physics, University of Paderborn, Warburger Straße 100, 33098 Paderborn, Germany*
[4]*Max-Planck-Institut für die Physik des Lichts, Günther-Scharowsky-Straße 1, Bau 24, 91058 Erlangen, Germany*
[5]*Departamento de Óptica, Facultad de Física, Universidad Complutense, 28040 Madrid, Spain*

We give a detailed account of an efficient search algorithm for the data pattern tomography proposed by J. Rehacek, D. Mogilevtsev, and Z. Hradil [Phys. Rev. Lett. **105**, 010402 (2010)], where the quantum state of a system is reconstructed without *a priori* knowledge about the measuring setup. The method is especially suited for experiments involving complex detectors, which are difficult to calibrate and characterize. We illustrate the approach with the case study of the homodyne detection of a nonclassical photon state.

PACS numbers: 03.65.Wj, 03.67.-a,02.60.Pn,42.50.Lc

Modern quantum technologies rely on the ability to create, manipulate, and measure quantum states. For the successful completion of these tasks, verification of each step in the experimental procedures is of utmost importance: quantum tomography has been developed for that purpose [1–3].

The main challenge of tomography is simple to state: given a finite set of identical copies of a system in a state represented by the density matrix ρ, and an informationally complete measurement [4], the state ρ must be inferred from the measured relative frequencies f_ℓ, which sample the true probabilities p_ℓ of distinct measurement outcomes. With these limited resources, the choice of optimal measurements and the design of efficient reconstruction algorithms turn out to be decisive.

The standard tomographic approach assumes a well-described measurement apparatus, that is, the responses $\rho \mapsto \{p_\ell\}$ to all the states in the search space can be determined. The issue of the independent characterization of detectors has recently started to attract a good deal of attention [5]. Quantum detector tomography employs the outcome statistics in response to a set of complete certified input states, at the cost of enlarging the set of unknown parameters from d^2 to d^4, in dimension d.

However, as shown in Ref. [6], if the measurement itself is of no interest, the costly detector calibration can be bypassed by using a direct fitting of data in terms of detector responses to input probes. Thus, state estimation is done without any prior knowledge of the measurement, avoiding unnecessary wasting of resources on appraising the parameters of the setup [7]. In addition, since all the information used is contained in the data patterns, the method is free of any assumption that cannot be verified experimentally. These substantial advantages have already been experimentally demonstrated [8].

The fitting of data patterns requires an optimization process with additional physical constraints (such as positivity). It is precisely the goal of this work to present a detailed implementation of a simple, robust, and efficient algorithm to perform such a job. This is an essential resource for any potential practitioner of this promising technique.

We recall that the central idea of the method is the possibility of expressing an arbitrary quantum signal ρ as a mixture,

$$\rho = \sum_{\xi}^{N} x_\xi \, \sigma_\xi \tag{1}$$

of N linearly independent (generally, nonorthogonal) states $\{\sigma_\xi\}$, with positive and negative weights $\{x_\xi\}$. We may look at (1) as some sort of discrete P representation.

An unknown measurement is mathematically interpreted as a set of positive operator-valued measures $\{\Pi_\ell\}$, with $\ell = 1,\ldots,M$ labeling the measurement outcomes [9]. The probability for detector outcome ℓ given input state σ_ξ is given by the Born rule $p_\ell^{(\xi)} = \mathrm{Tr}(\Pi_\ell \, \sigma_\xi)$. In a practical estimation with a finite number of copies, what we get is a frequency distribution $f_\ell^{(\xi)}$. By linearity, the response to an unknown signal ρ can be written as

$$\hat{f}_\ell = \sum_{\xi}^{N} x_\xi \, f_\ell^{(\xi)} . \tag{2}$$

Once the corresponding relative frequencies f_ℓ are measured, the coefficients x_ξ can be inferred and the signal reconstructed.

The goodness of the fit can be assessed with a variety of convex objective functions. In this work, we shall use the square distance

$$F(\{x_\xi\}) = \sum_{\ell}^{M} (f_\ell - \hat{f}_\ell)^2 , \tag{3}$$

which provides a robust least-squares fit. Consequently, we have to minimize the functional $F(\{x_\xi\})$ subject to $\rho \succeq 0$ and $\mathrm{Tr}(\rho) = 1$, which ensure that the reconstructed operator corresponds to a physical state.

The constraint $\mathrm{Tr}(\rho) = 1$ can be accounted for by noticing that it implies $x_N = 1 - \sum_{\xi}^{N-1} x_\xi$, which leaves us with $N-1$ independent variables we shall denote, for simplicity, by $\mathbf{x} =$

$(x_1,\ldots,x_{N-1}) \in \mathbb{R}^{N-1}$. To address the positivity, we employ a continuous function $c(\mathbf{x})$, such that $c(\mathbf{x}) \geq 0$ whenever $\rho(\mathbf{x}) \succeq 0$ and takes zero value at the boundary of the convex set of density matrices.

Fitting the data patterns thus takes the simplified form

$$\begin{aligned} \min_{\mathbf{x}} \quad & F(\mathbf{x}) \\ \text{subject to} \quad & c(\mathbf{x}) \geq 0\,. \end{aligned} \tag{4}$$

For a convex constraint $c(\mathbf{x})$, the primal problem (4) is convex and strictly feasible. The dual problem associated with Eq. (4) can be stated as [10, 11]

$$\begin{aligned} \max_{\lambda} \min_{\mathbf{x}} \quad & \mathscr{L}(\mathbf{x},\lambda) \\ \text{subject to} \quad & \lambda \geq 0\,, \end{aligned} \tag{5}$$

with $\mathscr{L}$ being the Lagrangian of (4)

$$\mathscr{L}(\mathbf{x},\lambda) = F(\mathbf{x}) - \lambda c(\mathbf{x})\,, \tag{6}$$

and λ being a dual variable. For strictly feasible convex problems, strong duality holds: the optimal of the Lagrange dual problem coincides with the minimum for the primal problem.

The complementary slackness condition ensures that at the local optimum x^* of (5) one has $\lambda c(\mathbf{x}^*) = 0$, and therefore the Lagrange multiplier must be zero when the constraint is not active at x^*. The complementary is perturbed by introducing a parameter μ

$$\lambda c(\mathbf{x}) = \mu\,, \tag{7}$$

to keep the search direction biased from the boundary.

The optimality conditions for (4) [or, equivalently, for (5)] are tantamount to including a logarithmic barrier function [10]; that is, instead of the constrained problem (4), one looks at the unconstrained version

$$\min_{\mathbf{x}} \quad F(\mathbf{x}) - \mu \log c(\mathbf{x})\,. \tag{8}$$

Given the properties of $c(\mathbf{x})$, the barrier term $\log c(\mathbf{x})$ goes to infinity as the point approaches the boundary of the feasible region. In this way, it penalizes points close to the border and thus ensures that one searches for an optimum well inside the region where the constraint is satisfied. The barrier parameter μ plays the role of a scaling factor: when it becomes very small the effect of the barrier becomes negligible within the strictly feasible set and only remains at the border.

By choosing a feasible starting point and gradually decreasing the height of the barrier, the optimal points of (8) will converge to the optimal points of the primal problem (4) from the interior regardless of the purity of the optimal state.

The extremal equations for the dual problem (5) read

$$g(\mathbf{x}) - \lambda J(\mathbf{x}) = 0\,, \tag{9}$$

along with the constraint (7). Here, $g(\mathbf{x}) = \nabla F(\mathbf{x})$ and $J(\mathbf{x}) = \nabla c(\mathbf{x})$ is the constraint Jacobian. There are a variety of numerical methods to solve (9), although the Newton search provides a particularly fast convergence. The Newton steps $\Delta_{\mathbf{x}}$ and Δ_λ of the primal and dual variables, respectively, obey

$$\begin{pmatrix} H & -J^T \\ \lambda J & c \end{pmatrix} \begin{pmatrix} \Delta_{\mathbf{x}} \\ \Delta_\lambda \end{pmatrix} = \begin{pmatrix} -g + \lambda J^T \\ \mu - \lambda c \end{pmatrix}, \tag{10}$$

where $H_{ij} = \partial^2 \mathscr{L}(\mathbf{x},\lambda)/\partial x_i \partial x_j$ is the Hessian matrix of the Lagrangian (6). To proceed further, we need to specify the function $c(x)$. Motivated by the barrier function $\log\det\rho(\mathbf{x})^{-1}$, which is strictly convex and analytical on the feasible space [12], and has been already employed in maximum likelihood estimations [13], we propose to adopt

$$c(\mathbf{x}) = \begin{cases} [\det\rho(\mathbf{x})]^m\,, & \rho(\mathbf{x}) \succeq 0\,, \\ 0, & \text{otherwise}\,, \end{cases} \tag{11}$$

where the parameter m ($0 < m < 1$) has been inserted to deal with the numerical issues that arise due to the extremely small values of $\det\rho$ near a highly rank-deficient optimum. Setting m to be the reciprocal of the Hilbert-space dimension $m = 1/d$ works well, and the algorithm is not very sensitive to small changes in this suggested value.

Using simple matrix identities, we get

$$\begin{aligned} J_i(\mathbf{x}) &\equiv \frac{\partial c(\mathbf{x})}{\partial x_i} = mc(\mathbf{x})\,\mathrm{Tr}(\Gamma_i), \\ B_{ij}(\mathbf{x}) &\equiv \frac{\partial^2 c(\mathbf{x})}{\partial x_i x_j} = c(\mathbf{x})^{-1} J_i J_j - mc(\mathbf{x})\,\mathrm{Tr}(\Gamma_i\Gamma_j), \end{aligned} \tag{12}$$

where we have denoted $\Gamma_i = \rho^{-1}(\sigma_i - \sigma_N)$.

With all these results in mind, we are ready to work out the desired solution. Our algorithm consists of outer and inner iterations; the latter solve (9) and (7) for a fixed value of μ. This value is gradually decreased to zero in outer iterations. In practice, only one inner iteration is done per outer iteration to increase the rate of convergence. The algorithm can be summarized in the following steps:

STEP 1: Choose $\mu \geq 0$ and $0 \leq \beta \leq 1$. Set $x_i = 1/N$ and $\lambda = \mu/c(\mathbf{x})$.

STEP 2: Solve the system (10) for the primal-dual steps $\Delta_{\mathbf{x}}$ and Δ_λ.

STEP 3: Set $\mathbf{x}' = \mathbf{x} + \alpha\Delta_{\mathbf{x}}$ and $\lambda' = \lambda + \alpha\Delta_\lambda$. Start from $\alpha = 1$ and backtrack α until $\rho(x') \succeq 0$, $\lambda' \geq 0$, and a sufficient decrease of the residuals of (9) is observed.

STEP 4: Decrease the barrier parameter $\mu = \beta\lambda' c(\mathbf{x}')$ and update the variables $\mathbf{x} = \mathbf{x}'$ and $\lambda = \lambda'$.

STEP 5: Repeat from STEP 2 until convergence.

Fine tuning of the algorithm can be achieved by altering the initial values of μ and β. Larger values tend to slow down the convergence, but improve stability. Typically, a few tens of iterations are required to solve a moderately sized problem (say, $d \approx 7$, $M \approx 80$, and $N \approx 100$).

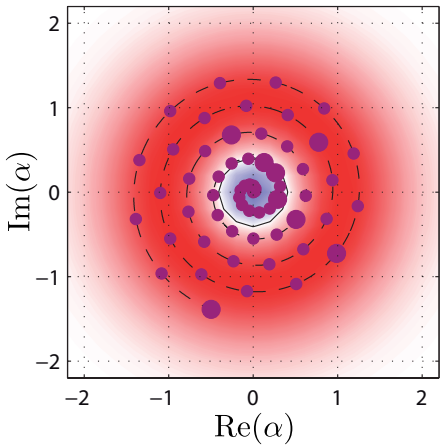

FIG. 1. (Color online) Amplitudes of coherent probes used to fit the data pattern in homodyne tomography. Probes 13, 15, 16, 25, 30, 40, 50, and 60 are marked with larger symbols. The density plot of the true $W(\alpha)$ is shown in the background: white represent zero of $W(\alpha)$, while the external part (red) and the internal one (blue) are the zones where $W(\alpha)$ is positive and negative, respectively.

The complexity of a single iteration depends on the parameters d, M, and N. Since there are at most $M-1$ linearly independent normalized patterns of size M, we can always set $N < M$. Three exclusive cases of interest can be identified:

1. Oversampled measurements: $M > \max(d^3, Nd^2, N^2)$. Setting up $\hat{f}_\ell$ and $\nabla F(\mathbf{x})$ dominates with cost $O(NM)$.

2. Informationally incomplete measurements: $N < d^2$. Setting up the constraint Hessian dominates with costs $O(Nd^3)$ and $O(N^2d^2)$ to generate all Γ_i's and carry out the pairwise inner products of Γ_i and Γ_j.

3. Informationally complete measurements: $N \geq d^2$. Solving the system (10) dominates with cost $O(N^3)$.

The complexity can be decreased by adopting a quasi-Newton approach [14] with a Broyden-Fletcher-Goldfarb-Shanno (BFGS) update of the Hessian matrix [case (2)] or a Hessian matrix inverse [case (3)] at the cost of slowing down the convergence [15].

To illustrate the utility of the proposed algorithm we examine the case of the homodyne measurement of a nonclassical photon state. We are then concerned with rotated-quadrature measurements $x(\theta) = x\cos\theta + p\sin\theta$, where x and p are the basic optical position and momentum observables and θ is the phase of the local oscillator. With a realistic detector efficiency of $\eta = 80$ %, the measurement consists of eigenvectors of $x(\theta)$ quadratures convolved with the vacuum. Explicit formulas for the measurement operators in the computational Fock basis can be found, e.g., in Ref. [16]. We discretize the measurement using six equidistant phases and 61 quadrature value bins in the interval $x \in [-6, 6]$. Each of these six quadratures is measured 200000 times for each different state, with the data being drawn from the multinomial distribution describing the measurement statistics.

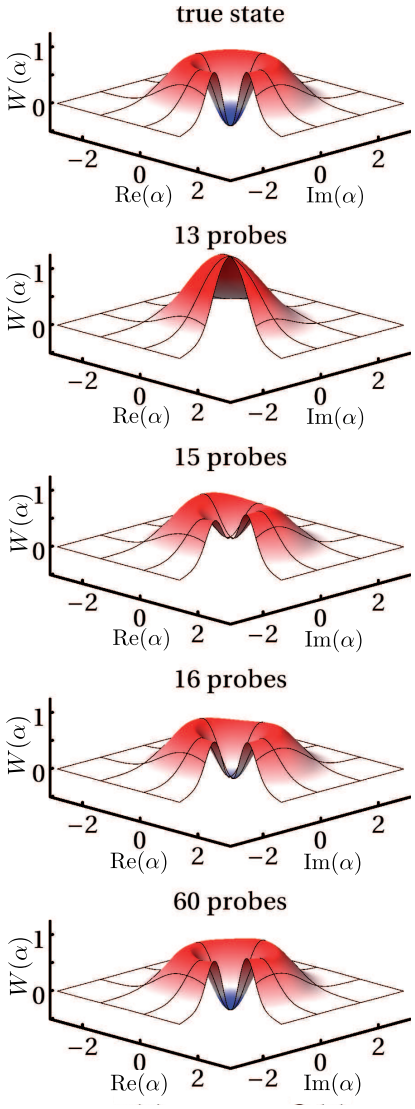

FIG. 2. (Color online) True vs. reconstructed Wigner functions for different number of coherent probes. All the reconstructions have been performed in an eight-dimensional Fock subspace.

As a signal state, we have simulated an incoherent mixture $\rho_{\text{true}} = 0.4|0\rangle\langle 0| + 0.6|1\rangle\langle 1|$ of vacuum and a single-photon state, which can be prepared in parametric downconversion [17]. The pronounced negativity of the corresponding Wigner function at the origin is a nonclassicality witness and will be a test for our scheme. As with every genuine quantum feature, it is rather sensitive to tomography imperfections.

In our simulation, this state is measured together with a set of known coherent probe states $\sigma_i = |\alpha_i\rangle\langle\alpha_i|$, which are robust and easy to generate on demand. The coherent amplitudes are sampled from a spiral pattern unwinding from the origin, as sketched in Fig. 1. The resulting samples are equidistant in radius and angle, but other choices, such as a rectangular grid, would work as well.

Without *a priori* knowledge of the true state, one might think of sampling the phase space starting from the origin and

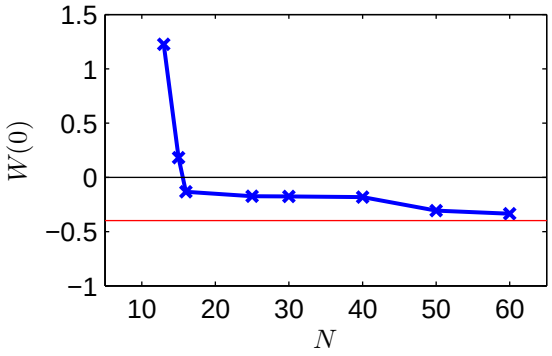

FIG. 3. (Color online) Reconstructed Wigner functions evaluated at the origin, $W(0)$, with 13, 15, 16, 25, 30, 40, 50, and 60 coherent probes, as in Fig. 1. The quantum/classical border, $W(0)=0$, and the true negative value $W(0)=-0.4$ are indicated by horizontal lines.

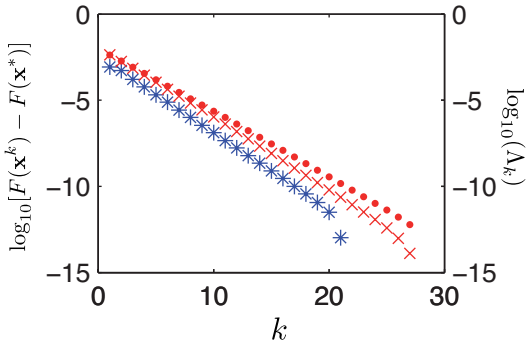

FIG. 4. (Color online) Convergence of the algorithm with 15 (blue stars) and 60 probes (red crosses). $F(\mathbf{x}^*)$ is the exact value at the optimal point, while $F(\mathbf{x}^k)$ is the calculated value after the kth iteration. For the later case, we have also included $\log(\Lambda^k)$ (in the right vertical axis), where Λ^k denotes the minimal eigenvalue of $\rho(\mathbf{x}^k)$. Observe how the state converges towards the boundary of the space of density matrices. The parameters are $\mu=0.01$, $\beta=0.1$, $m=1/6$ and decimal logarithm is used everywhere.

gradually increasing the size of the probe set until no significant updates of the reconstruction are observed. This strategy is illustrated in Fig. 2, which shows the reconstructed Wigner function for different numbers of coherent probes. Notice that 13 probes yield a classical state whose Wigner function peaks near the origin. The central dip develops with 15 probes, and just 16 probes are enough to observe negativities. Finally, with 60 probes the reconstruction becomes nearly perfect, with some residual errors due to unavoidable statistical noise. The reconstructed $W(\alpha)$ becomes smoother and circularly symmetrical with larger probe sets, increasing thus the overall fidelity of the protocol [the fidelity $\mathscr{F}=\mathrm{Tr}(\sqrt{\sqrt{\rho_{\mathrm{true}}}\rho\sqrt{\rho_{\mathrm{true}}}})$ of the reconstruction with 60 probes is 99.2 %].

In Fig. 3 we plot the reconstructed value of $W(0)$ as a function of the probe set size N. It is intriguing to observe that the abrupt drop of $W(0)$ for $N\sim 16$ arises when the probe amplitudes reach the edge of the negative region of the true Wigner function, as can be seen in Fig. 1. Furthermore, the drop of $W(0)$ between $N=40$ and $N=50$ seems to happen at the point where the coherent probes pass the maximum of W and start to feel the region in which the true Wigner function decays to zero.

In Fig. 4 we depict the convergence of the algorithm for the simulated data in Fig. 2. A slight increase in the number of iterations with the problem size is observed, as might be expected.

Last, in Fig. 5 we present typical fidelities of data pattern tomography for states of varying purity. The variations of the fidelity observed are not statistically significant.

We stress that our knowledge about the measurement was used solely for generating data. The pattern tomography itself was based on the signal data, probe data and the representation of probes in the computational basis. In this way, the search space —the field of view of tomography— was defined uniquely by the measured objects, avoiding the problematic *ad hoc* Hilbert space truncation of the standard methods [18].

In summary, we have re-elaborated on the data pattern approach to quantum tomography. The most relevant feature of the approach is the ability to perform an efficient reconstruction without ever knowing the exact properties of the measurement setup. The knowledge required for the precise estimation of a particular signal state can be obtained a posteriori, after the measurement on the signal state. One can also decide which additional probes might be helpful in further improving the reconstruction. This is a significant advantage for experimentalists, since calibrating the measurement setups for such weak signals can be a rather challenging task.

This work was supported by the European Social Fund and the State Budget of the Czech Republic POSTUP II (Grant CZ.1.07/2.3.00/30.0041) and MCIN (Grant CZ.1.07/2.3.00/20.0060), the IGA Project of the Palacký University (Grant PRF 2013 019), the Spanish MINECO (Grant FIS2011-26786), and the External Fellowship Program of the Russian Quantum Center at Skolkovo. We acknowledge illuminating discussions with A. Felipe.

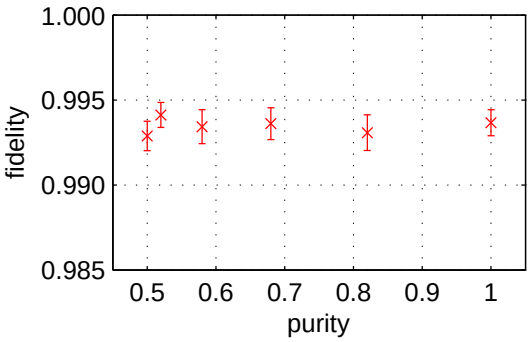

FIG. 5. (Color online) Mean fidelities of data pattern reconstruction with true states $\rho_{\mathrm{true}}=0.5|0\rangle\langle 0|+0.5|1\rangle\langle 1|+\gamma|0\rangle\langle 1|+\gamma|1\rangle\langle 0|$, $\gamma\in[0,0.5]$ of different purities measured by $\mathrm{Tr}(\rho^2_{\mathrm{true}})$. The averaging was done over 50 runs of simulated homodyne detection with 60 probes. Standard deviations of those 50 fidelities are also shown.

[1] M. G. A. Paris and J. Řeháček, eds., *Quantum State Estimation*, Lect. Not. Phys., Vol. 649 (Springer, Berlin, 2004).

[2] I. Chuang and M. Nielsen, *Quantum Computation and Quantum Information* (Cambridge University Press, Cambridge, 2000).

[3] U. L. Andersen, G. Leuchs, and C. Silberhorn, Laser Photonics Rev. **4**, 337 (2010).

[4] E. Prugovečki, Int. J. Theor. Phys. **16**, 321 (1977); P. Busch and P. J. Lahti, Found. Phys. **19**, 633 (1989); G. M. D. Ariano, P. Perinotti, and M. F. Sacchi, J. Opt. B **6**, S487 (2004); S. T. Flammia, A. Silberfarb, and C. M. Caves, Found. Phys. **35**, 1985 (2005); S. Weigert, Int. J. Mod. Phys. B **20**, 1942 (2006).

[5] A. Luis and L. L. Sánchez-Soto, Phys. Rev. Lett. **83**, 3573 (1999); J. Fiurášek, Phys. Rev. A **64**, 024102 (2001); G. M. D'Ariano, L. Maccone, and P. Lo Presti, Phys. Rev. Lett. **93**, 250407 (2004); J. S. Lundeen, A. Feito, H. Coldenstrodt-Ronge, K. L. Pregnell, C. Silberhorn, T. C. Ralph, J. Eisert, M. B. Plenio, and I. A. Walmsley, Nat. Phys. **5**, 27 (2009); T. Amri, J. Laurat, and C. Fabre, Phys. Rev. Lett. **106**, 020502 (2011); L. Zhang, A. Datta, H. B. Coldenstrodt-Ronge, X.-M. Jin, J. Eisert, M. B. Plenio, and I. A. Walmsley, New J. Phys. **14**, 115005 (2012); G. Brida, L. Ciavarella, I. P. Degiovanni, M. Genovese, L. Lolli, M. G. Mingolla, F. Piacentini, M. Rajteri, E. Taralli, and M. G. A. Paris, *ibid*. **14**, 085001 (2012); C. M. Natarajan, L. Zhang, H. Coldenstrodt-Ronge, G. Donati, S. N. Dorenbos, V. Zwiller, I. A. Walmsley, and R. H. Hadfield, Opt. Express **21**, 893 (2013).

[6] J. Řeháček, D. Mogilevtsev, and Z. Hradil, Phys. Rev. Lett. **105**, 01040 (2010).

[7] D. Mogilevtsev, A. Ignatenko, A. Maloshtan, B. Stoklasa, J. Rehacek, and Z. Hradil, New J. Phys. **15**, 025038 (2013).

[8] M. Cooper, M. Karpinski, and B. J. Smith, arxiv:1306.6431 .

[9] C. W. Helstrom, *Quantum Detection and Estimation Theory* (Academic, New York, 1976).

[10] A. Forsgren, P. E. Gill, and M. H. Wright, SIAM Rev. **44**, 525 (2002).

[11] S. Boyd and L. Vandenberghe, *Convex Optimization* (Cambridge University Press, Cambridge, 2004).

[12] L. Vandenberghe and S. Boyd, SIAM Rev. **38**, 49 (1996).

[13] T. Moroder, P. Hyllus, G. Tóth, C. Schwemmer, A. Niggebaum, S. Gaile, O. Gühne, and H. Weinfurter, New J. Phys. **14**, 105001 (2012).

[14] R. Fletcher, *Practical Methods of Optimization*, 2nd ed. (Wiley, Chichester, 1987).

[15] P. Armand, J.-C. Gilbert and S. Jan-Jégou, *A Feasible BFGS Interior Point Algorithm for Solving Strongly Convex Minimization Problems*, Tech. Rep. (Université de Limoges, 2001).

[16] A. I. Lvovsky, J. Opt. B **6**, S556 (2004).

[17] K. Laiho, K. N. Cassemiro, D. Gross, and C. Silberhorn, Phys. Rev. Lett. **105**, 253603 (2010).

[18] D. Mogilevtsev, Z. Hradil, J. Rehacek, and V. S. Shchesnovich, Phys. Rev. Lett. **111**, 120403 (2013).